Electronic Supplementary Material (ESI) for Journal of Materials Chemistry A.

Supporting Information

Effect of Proton Irradiation on Electrocatalytic Properties of MnO_2 for Oxygen Reduction Reaction

Yeji Choi, Dongwook Lim, Euntaek Oh, Chaewon Lim, and Sung-Hyeon Baeck*

Department of Chemistry and Chemical Engineering, Center for Design and Applications of Molecular Catalysts, Inha University, Incheon 22212, Korea

*E-mail address: shbaeck@inha.ac.kr

Experimental Procedures

Chemicals

The activated MnO_2 powder was purchased from Sigma-Aldrich. The 20 wt% Pt/C was obtained from Alfa Aesar. High purity oxygen and nitrogen were used in this study and all chemicals were used without further purification.

Proton irradiation

Two methods of preparing MnO_2 for proton irradiation were performed; evenly spreading commercial MnO_2 powder with an area of 30 mm × 30 mm and a thickness of 0.65 mm and ultrasonically dispersing 250 mg of the powder into 2 mL of deionized water. Both types of MnO_2 were irradiated with 5 and 14 MeV protons at a fixed fluence of 5.0×10^9 protons cm^{-2} $purse^{-1}$. The protons were accelerated to 20 MeV using TR23 at Korea Multi-purpose Accelerator Complex (KOMAC), reaching the targets with 5 and 14 MeV of energy by adjusting the thickness of the aluminum degraders. During irradiation, the average peak current of the proton beam was 4 mA and the total dose was maintained at 5 kGy. The samples are named in the following format: MnO_2-energy-proton-preparation-type. The MnO_2 proton irradiated at 14 MeV was used for detailed studies.

Physicochemical characterization

The morphology of the proton-beam-treated samples was characterized by scanning electron microscopy (SEM; Hitachi, S-4300SE) and high resolution transmission electron microscopy (HR-TEM; JEOL, JEM2100F). The crystal structures and crystallinity of the catalysts were examined by X-ray diffraction (XRD; Rigaku, D/max-2200). The surface oxygen compositions of the prepared samples were determined by X-ray photoelectron spectroscopy (XPS; Thermo Scientific, K-Alpha). The specific surface area of samples was investigated by Brunauer-Emmett-Teller (BET) analysis (Micromeritics, ASAP 2020). The oxygen vacancy concentration of the prepared catalysts was obtained by thermogravimetric analysis (TGA; PerkinElmer, TGA 4000). The average oxidation state of Mn was calculated from the XPS O 1s data using the following equation with some modification.[1]

$$Oxidation\ state\ of\ Mn = \frac{\left[IV \times \left(S_{Mn-O-Mn} - S_{Mn-OH} - S_{oxygen\ defect}\right) + III \times \left(S_{Mn-OH} + S_{oxygen\ defect}\right)\right]}{S_{Mn-O-Mn}}$$

where S denotes the corresponding O 1s spectrum peak area. The original equation was computed with two O 1s components, the metal-oxygen bond (Mn-O-Mn) and that of the hydroxyl group (Mn-OH). In this study, the equation included the oxygen defect site signal related to the Mn(III) species. The oxygen vacancy concentration of the proton-irradiated MnO_2 samples was calculated from TGA weight loss difference under oxygen and nitrogen atmosphere. The substoichiometry concentration x was calculated from the following equation.[2]

$$M_w(MnO_2) = (1 + [(\%\ mass\ loss/gain\ in\ O_2) - (\%\ mass\ loss/gain\ in\ N_2)]/100) \times M_w(MnO_{2-x})$$

Electrochemical tests

The electrochemical experiments were performed in a three-electrode system composed of a platinum wire, glassy carbon (GC), rotating disk (RDE, 3 mm in diameter), and Ag/AgCl/KCl (3 M) electrodes as counter, working, and reference electrodes, respectively. The working electrode was prepared by dispersing 0.89 mg of the catalyst, 1.11 mg of Ketjen black, and 16 μL of Nafion solution (5 wt%) into 100 μL of iso-propanol and 384 μL of deionized water with a resistivity of 18.2 MΩ. A 5 μL drop of catalyst ink was applied onto the GC electrodes (3.0 mm in diameter) and dried naturally. Prior to ink deposition, the GC electrode was polished with aqueous alumina suspensions on felt polishing pads, followed by ultrasonic cleaning. The electrochemical characterizations of the prepared electrodes were conducted by cyclic voltammetry (CV) and linear sweep voltammetry (LSV) in 0.1 M aqueous KOH bubbled with O_2 gas for more than 30 min prior to the measurements. The voltammetry experiments were investigated from 1.3 to 0 V (vs. RHE) at a sweep rate of 100 mV s^{-1} for CV and 5 mV s^{-1} for LSV using a potentiostat (Princeton Applied Research, VSP). The electron transfer numbers (n) for the ORR were calculated based on the Koutecky-Levich equation :

$$\frac{1}{J} = \frac{1}{J_K} + \frac{1}{J_D} \tag{1}$$

$$J_D = 0.62nFD^{2/3}v^{-1/6}\omega^{1/2}C_{O_2} \tag{2}$$

where J is the measured current density, J_K is the kinetic current density, and J_D is the diffusion limiting current density, n is the number of transferred electrons, F is the Faraday constant (96485 C mol^{-1}), D is the diffusion coefficient of O_2 in 0.1 M KOH (1.93×10^{-5} cm^2 s^{-1}), v is the kinematic viscosity of the electrolyte (1.09×10^{-2} cm^2 s^{-1}), w is the angular frequency of rotation ($\omega = 2\pi f/60$, f is the rotating speed of RDE), and $C_{O_2}$is the oxygen concentration in 0.1 M KOH (1.26×10^{-6} mol cm^{-3}). For the Tafel plot, the kinetic current density was calculated using the mass transfer-correction of the RDE :

$$J_K = \frac{J \times J_D}{(J_D - J)} \tag{3}$$

Stability testing was conducted by current-time chronoamperometry (CA) measurements at 0.6 V (vs. RHE) for 10000 s.

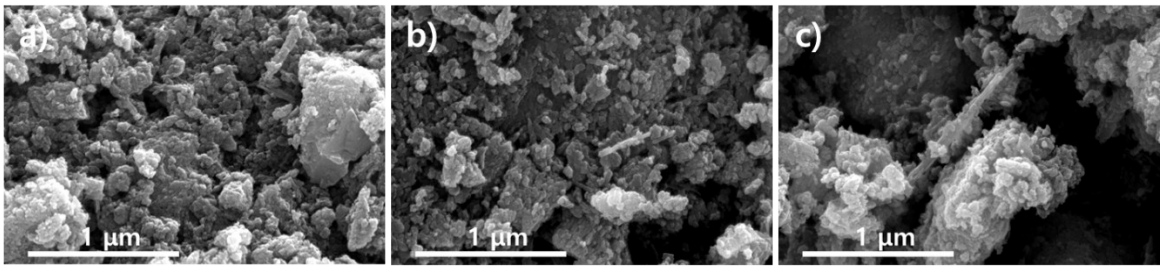

Fig. S1 SEM images of (a) pristine MnO_2, (b) MnO_2-5MeV-pwd, and (c) MnO_2-5MeV-sol.

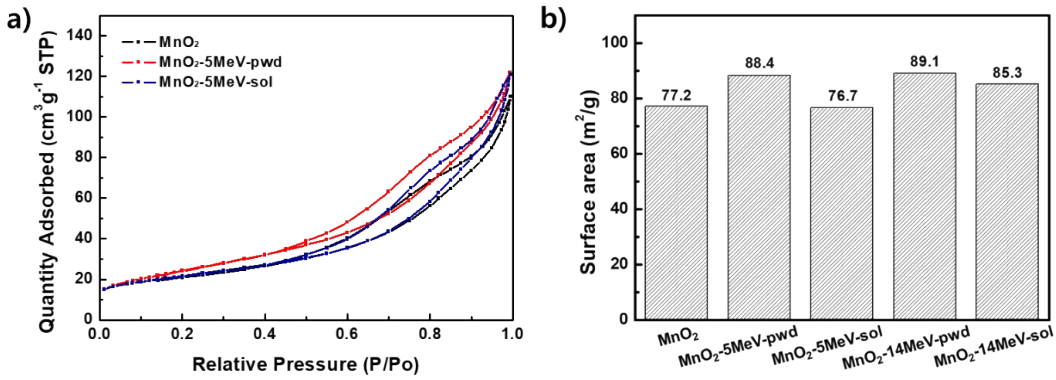

Fig. S2 (a) N_2 sorption isotherms of MnO_2, MnO_2-5MeV-pwd, and MnO_2-5MeV-sol. (b) BET surface areas of MnO_2, MnO_2-5MeV-pwd, MnO_2-5MeV-sol, MnO_2-14MeV-pwd, and MnO_2-14MeV-sol.

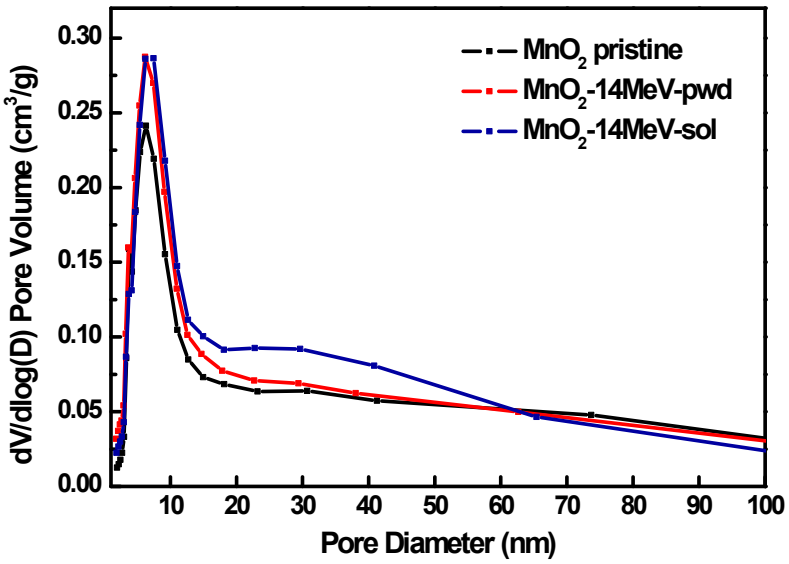

Fig. S3 BJH pore size distribution curves of MnO_2, MnO_2-14MeV-pwd, and MnO_2-14MeV-sol.

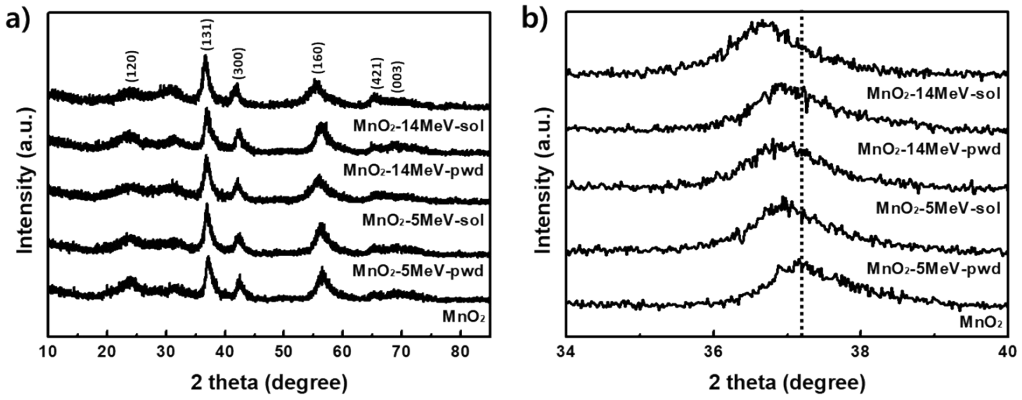

Fig. S4 (a) XRD patterns of MnO_2, MnO_2-5MeV-pwd, MnO_2-5MeV-sol, MnO_2-14MeV-pwd, and MnO_2-14MeV-sol. (b) Enlarged region of the MnO_2 (131) diffraction peaks from (a).

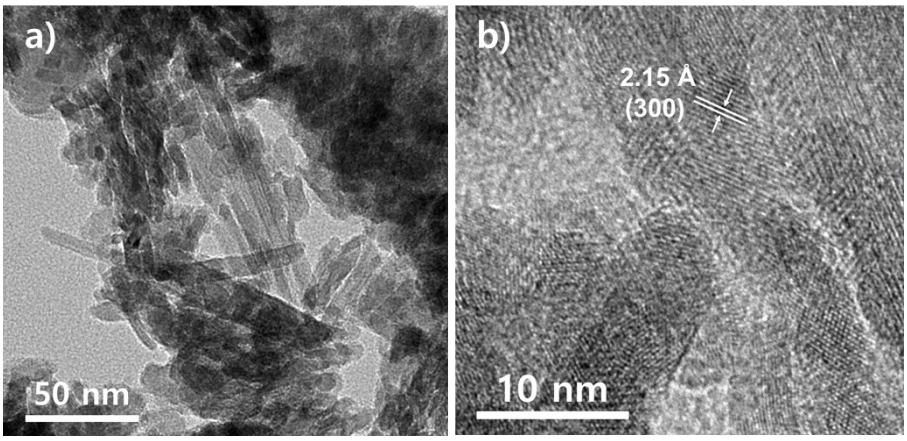

Fig. S5 (a) TEM image and (b) high-magnification HRTEM image of MnO_2-14MeV-sol.

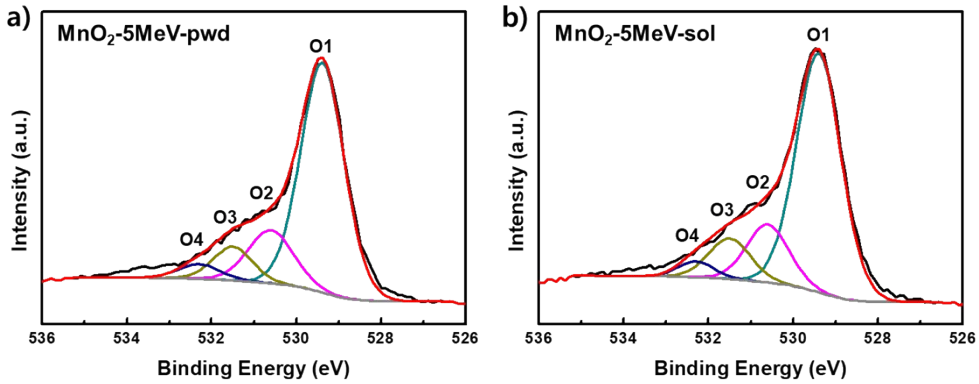

Fig. S6 Fitted O 1s spectra of (a) MnO_2-5MeV-pwd and (b) MnO_2-5MeV-sol.

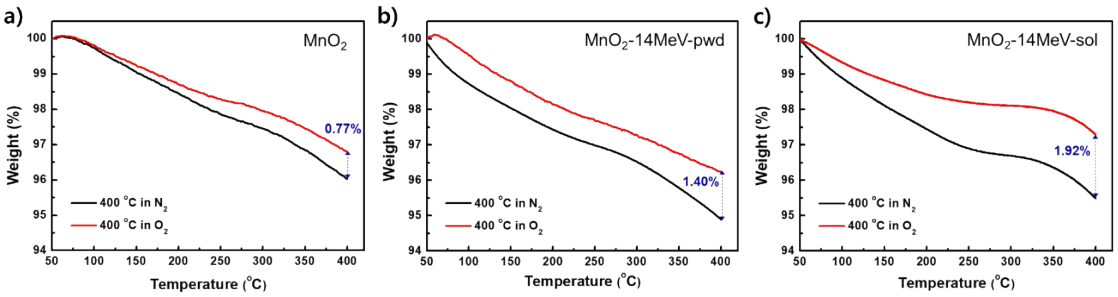

Fig. S7 Thermogravimetric analysis (TGA) of (a) MnO_2, (b) MnO_2-14MeV-pwd, and (c) MnO_2-14MeV-sol in nitrogen and oxygen atmosphere. TGA was performed from 50–400 ℃ at a heating rate of 10 ℃ min^{-1} and a flow rate of 10 sccm. The x value of MnO_{2-x} is calculated from the above equation in experimental procedures.

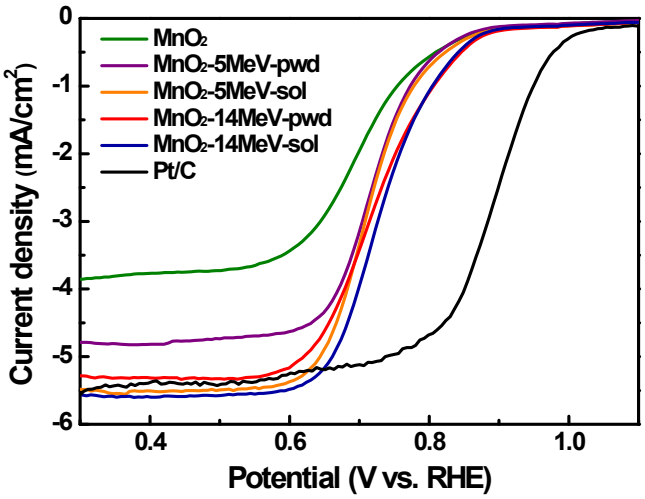

Fig. S8 LSV curves of proton-irradiated MnO_2 samples in O_2-saturated 0.1 M KOH for the ORR.

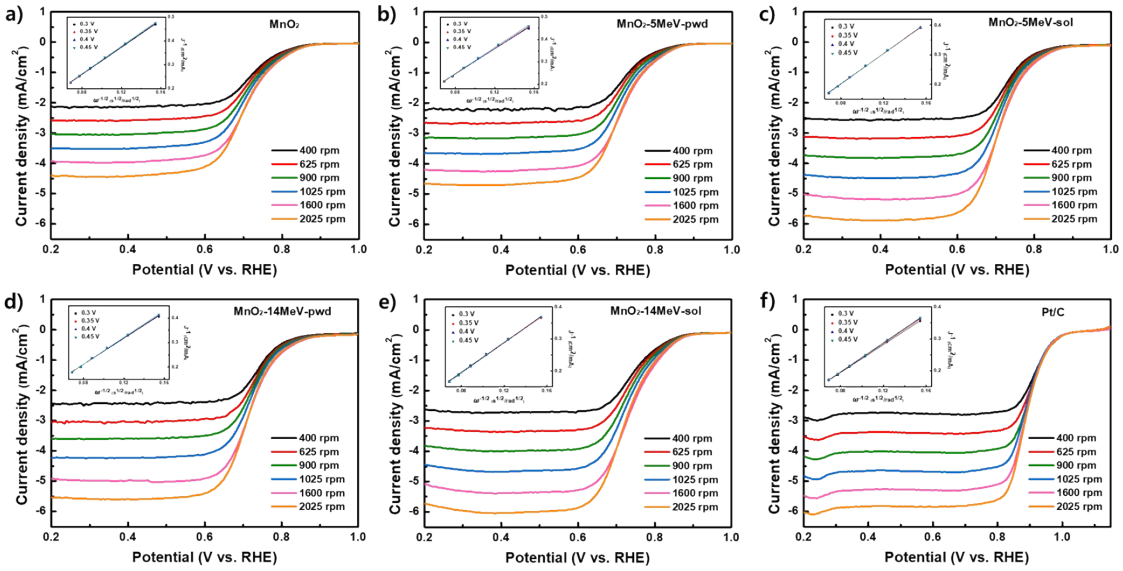

Fig. S9 Rotating disk voltammograms of (a) MnO_2, (b) MnO_2-5MeV-pwd, (c) MnO_2-5MeV-sol, (d) MnO_2-14MeV-pwd, (e) MnO_2-14MeV-sol, and (f) Pt/C. The insets of (a)-(f) show Koutecky-Levich plots at potentials from 0.3-0.45 V.

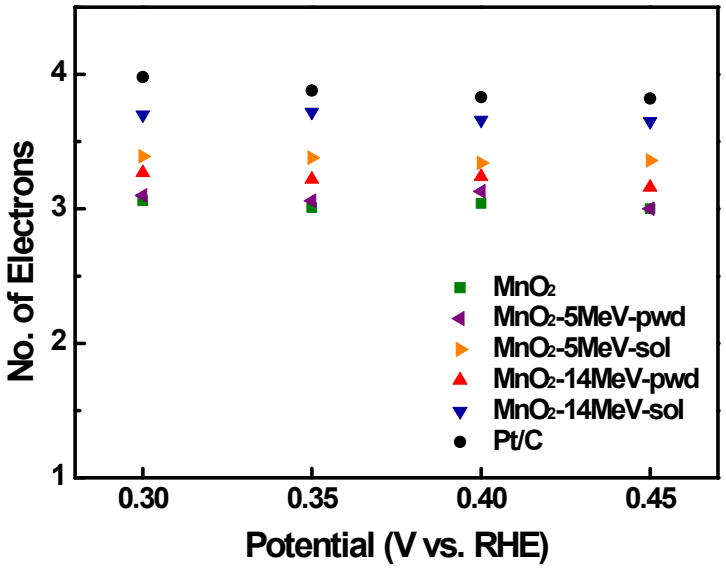

Fig. S10 Electron transfer number of proton-irradiated MnO_2 catalysts as a function of applied voltage.

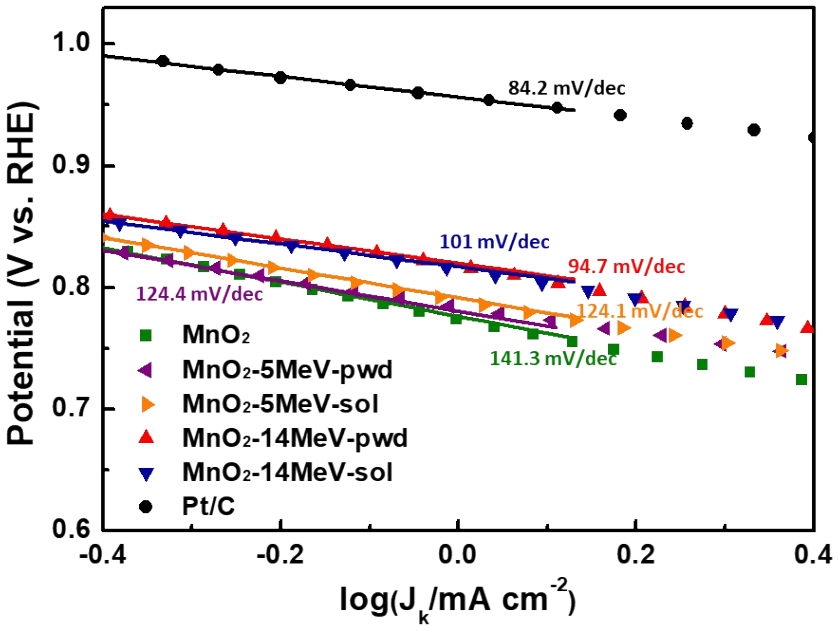

Fig. S11 Tafel plots of MnO_2 catalysts under various proton irradiation conditions for the ORR obtained by mass-transport-correction.

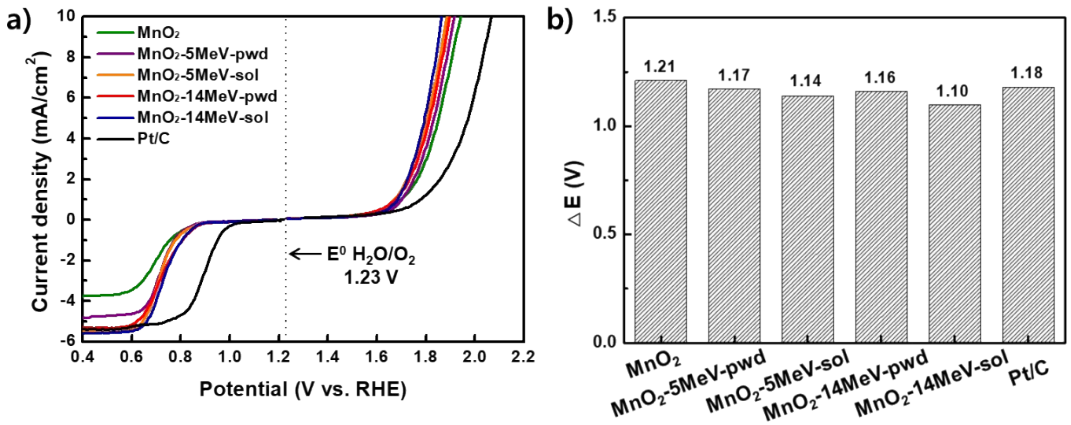

Fig. S12 (a) Overall oxygen electrode activities of the catalysts within the ORR and OER potential window in O_2-saturated 0.1 M KOH. (b) ΔE values of the proton-irradiated MnO_2 and Pt/C catalysts ($\Delta E = E_{j10} - E_{1/2}$).

Table S1. Area ratio of the O 1s components for the proton-irradiated MnO_2.

Samples	O1	O2	O3	O4	Mn oxidation state
MnO_2	70.3	18.8	6.8	4.1	3.64
MnO_2-5MeV-pwd	69.5	16.9	9.3	4.3	3.62
MnO_2-5MeV-sol	69.1	16.0	11.1	3.8	3.61
MnO_2-14MeV-pwd	69.7	16.6	10.2	3.5	3.62
MnO_2-14MeV-sol	66.5	18.1	11.9	3.5	3.55

Table S2. Detailed information for the ORR catalytic activities of the MnO_2-based samples.

Number	Catalyst	Overpotential (V vs. RHE)	Half-wave potential (V vs. RHE)	Diffusion-limiting current density (mA cm^{-2})	Ref.
1	MnO_2 nanoflakes	0.448	0.666	-4.8	3
2	MnO_2 large particles	0.49	0.645	-4.5	3
3	Tremella-shaped MnO_2	0.39	0.758	-3.05	4
4	Mixed tremella-nanobelt MnO_2	0.38	0.75	-4.0	4
5	Nanobelt-shaped MnO_2	0.328	0.771	-4.02	4
6	ε-MnO_2 + MOF(Fe)	0.487	0.6515	-4.9	5
7	ε-MnO_2/MOF(Fe)	0.44	0.675	-5.0	5
8	Hydrogenated H-MnO_2 2h	0.36	0.77	-3.59	6
9	Hydrogenated H-MnO_2 24h	0.355	0.7725	-3.85	6
10	Hydrogenated H-MnO_2 72h	0.36	0.77	-3.59	6
11	β-MnO_2 Air-250 ℃-2h annealing	0.373	0.6985	-5.38	7
12	β-MnO_2 Air-400 ℃-2h annealing	0.38	0.695	-5.37	7
13	β-MnO_2 Air-450 ℃-2h annealing	0.38	0.695	-5.2	7
14	λ-MnO_{2-z} 750 ℃ calcination	0.433	0.7135	-3.94	8
15	λ-MnO_{2-z} 900 ℃ calcination	0.425	0.7175	-4.75	8
16	λ-MnO_{2-z} 1050 ℃ calcination	0.425	0.6965	-5.4	8
17	MnO_2-5MeV-pwd	0.38	0.7475	-4.84	This work
18	MnO_2-5MeV-sol	0.38	0.745	-5.5	This work
19	MnO_2-14MeV-pwd	0.365	0.745	-5.3	This work
20	MnO_2-14MeV-sol	0.365	0.7525	-5.6	This work

References

1. M. Toupin, T. Brousse and D. Bélanger, *Chem. Mat.,* 2004, **16**, 3184.
2. S. Yazdani, R, Kashfi-Sadabad, T. D. Huan, M. D. Morales-Acosta and M. T. Pettes, *Langmuir,* 2018, **34**, 6296.
3. C. Wei, L. Yu, C. Cui, J. Lin, C. Wei, N. Mathews, F. Huo, T. Sritharan and Z. Xu, *Chem. Commun.,* 2014, **50**, 7885.
4. Y. Ma, R. Wang, H. Wang, J. Key and S. Ji, *J. Power Sources,* 2015, **280**, 526.
5. H. Wang, F. Yin, B. Chen and G. Li, *J. Mater. Chem. A,* 2015, **3**, 16168.
6. T. Zhang, F. Cheng, J. Du, Y. Hu and J. Chen, *Adv. Energy Mater.,* 2015, **5**, 1400654.
7. F. Cheng, T. Zhang, Y. Zhang, J. Du, X. Han and J. Chen, *Angew. Chem. Int. Ed.,* 2013, **52**, 2474.
8. S. Lee, G. Nam, J. Sun, J. S. Lee, H. W. Lee, W. Chen, J. Cho and Y. Cui, *Angew. Chem. Int. Ed.,* 2016, **55**, 8599.